Flexible Actuation with Intrinsic Sensing for Ram Extrusion 3D Printing

Setthibhak Suthithanakom[1], Chaiwuth Sithiwichankit[1†], Kantawatchr Chaiprabha[1†], Ratchatin Chancharoen[1*†]

[1*]Department of Mechanical Engineering, Chulalongkorn University, 254 Phaya Thai Road, Bangkok, 10330, Thailand.

*Corresponding author(s). E-mail(s): ratchatin.c@chula.ac.th;
Contributing authors: setthibhak@gmail.com; chaiwuth.cs@gmail.com; kant.chai@gmail.com;
[†]These authors contributed equally to this work.

Abstract

This paper introduces a flexible actuation system with intrinsic sensing for ram extrusion 3D printing, enabling the control of extrusion flow in both pressure and volumetric modes. The system incorporates real-time monitoring of extrusion pressure and flow rate, allowing precise control and adjustment proceeded during the printing process. In addition to extrusion-flow control, the system has the capability to detect printing-material properties, such as viscosity, providing valuable insights for further optimization of the printing process. The proposed system offers the advantages of improved pressure and flow control, as well as the ability to monitor and adapt to printing-material properties. In conclusion, the contribution of this paper enhances the overall performance and efficiency of ram extrusion in 3D printing.

Keywords: Liquid Deposition Modelling, Ram Extrusion, Actuation and Sensing, Viscoelastic Material

1 Introduction

Liquid Deposition Modeling (LDM), also known as Direct Ink Wiring (DIW) is an advanced form of 3D printing that utilizes liquid or gel-like materials as the primary medium for creating three-dimensional objects [1], [2]. This fabrication process features most of the benefits of additive manufacturing. Furthermore, it supports a wide range of materials [3], including polymers [4], [5], ceramics [6], [7], metals [8], [9], and even biological materials like hydrogels [10], [11]. This versatility makes it applicable across various industries [1], each with unique material requirements.

One of the significant potential industries is Bioprinting and Tissue Engineering where this technique can precisely deposit living cells and biomaterials to create functional tissue structures for transplantation or research purposes [11], [12]. There are several collaborative research and developments around this technique that work towards a reliable and precise fabrication process. The scope of this technique includes (a) biomaterial for functional tissues and organs [2], [10], (b) material extrusion that precisely controls the flow of material including in situ parameters [13], (c) curing and solidification [14], and (d) post-processing [15].

For the research and development in advanced 3D printing of biomaterials toward various tissues and organs, one of the remarkable difficulties is that biomaterials must mimic complex living tissues while their properties are also expected to favor the 3D printing process [16]. In general, biomaterials are mixtures of living cells and hydrogel-like substances. Such materials physically perform like viscoelastic materials [2], which exhibit the characteristics of both elastic solid and viscous fluid.

To achieve the desired structures of biomaterial, it must be deposited with an accurate amount. Extrusion flow is necessary to be precisely controlled for this purpose. However, the mechanical properties of biomaterials trend to priori unknown and vary during the 3D printing process. There are three common approaches for extrusion gel-like materials including, pneumatic actuation, piston actuation, and screw actuation. The pneumatic actuation method relies on the fundamentals of controlling the printing pressure through compressed air. This provides reliable extrusion flow only if biomaterials have narrow variations in mechanical properties. To handle those materials with larger property variation, piston actuation has been employed together with the concept of motion control on pistons. The common forms of piston actuation are to drive the lead screw or ball screw by a stepper motor [17]. When the rotation motion is applied, the piston is pushed and the material is extruded. This allows the flow to be reliably obtained in a steady state. Screw actuation performs similarly by precisely controlling the flow by the rotation of the screw. Screw actuation gains benefit over the piston by allowing the extrusion of highly viscous material [8].

Despite the success in flow control for these two positive displacement actuations, extrusion flow in a transient state cannot be controlled deterministically. The viscoelasticity of biomaterials plays a key role in this challenge. Due to the elastic behavior of the material, pressure manipulation is required to gain control over the flow. Further studies are required to overcome this problem.

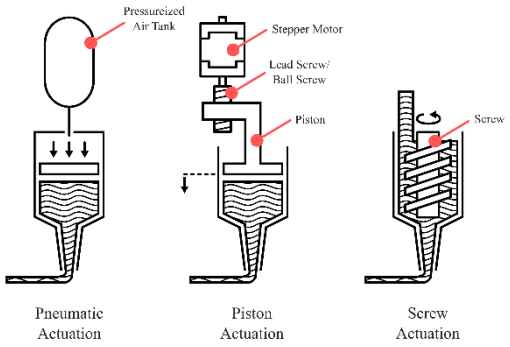

Fig 1 Types of actuation technique. First, pneumatic actuation utilizes the pressurized air in the tank to push the material. Second, in the piston actuation, the stepper motor and lead screw/ball screw are used to displace the piston. Third, screw actuation uses a rotating screw to directly displace the material.

This research presents the development of a novel piston-driven material extruder with the features of flexible actuation and intrinsic sensing. Basically, flexible actuation refers to the concept of controlling either extrusion pressure or volumetric flow, one at a time. The context of intrinsic sensing is the perception of the mechanical properties of biomaterials during the extrusion, together with the pressure and flow rate which are the critical keys for the printing process.

This type of actuation proposes the possibility of control over the extrusion of materials that are not specifically tuned for 3D printing.

Mathematic analysis, simulation, and experiments were used to demonstrate the benefits of the proposed design. The flexible actuation provides control over the whole extrusion process, with pressure-controlled for transient state handling and volumetric-controlled for precise extrusion in the steady state. Intrinsic sensing not only be the foundation of the flexible actuation but also further enhances the performance of this design. By enabling real-time material properties sensing, many useful features could be developed and implemented in the process. For example, on-the-fly detection of anomalies such as clogging, bubbles, and sediment.

2 Methodology

2.1 Modelling Ram-Extruder

The proposed ram extrusion was designed to effectively control the flow of the printing material in two modes: either (1) pressure or (2) volumetric flow control. If the ram extruder is under pressure control, the volumetric flow rate can be monitored. Vice versa, if the ram extruder is in volumetric flow control, the pressure inside the syringe can be monitored. The printing material is viscoelastic and suitable for three-dimensional printing with the technique of liquid deposition modeling. The actuator, for the ram extrusion, is commanded by a control signal and can provide sufficient force to extrude the material out of the syringe. In this case, a permanent magnet DC motor is preferred, compared to a stepper motor. This is because the motor model is less complex, and the flexible control mode can be implemented as described in the section. Consider the governing equations of this motor as follows.

Table 1 Nomenclature

Symbols	Values	Unit	Description
R_m	4	Ω	Motor Resistance
L_m	99.5	μH	Motor Inductance
K_V	0.0261	V·s/rad	Motor Velocity Constant
K_T	0.0261	N·m/A	Motor Torque Constant
J	0.001	kg·m^2	System Moment of Inertia
f	30	N	System Friction
r	0.001	m	Screw Radius
α	4.55	deg	Lead Angle
μ	0.05	N/A	Screw Friction Coefficient
D	0.0148	m	Syringe Inner Diameter
M		kg	Carriage Mass
m	N/A	kg	Material Mass
k	N/A	N/m	Material Spring Constant
c	N/A	N·s/m	Material Damping Coefficient

Table 2 Variables

Symbols	Unit	Description
X_1	m	Displacement of Piston
X_2	m	Displacement of Material Entering Nozzle
θ	rad	Angular Displacement of Screw
ω	rad/s	Angular Velocity of Screw
V	V	Voltage
I	A	Current
T	N·m	Motor Torque
F	N	Screw Load
P	Pa	Syringe Pressure
Q	m^3/s	Volumetric Flow Rate

A controllable voltage source applies a voltage, V, to a permanent magnet DC motor. The electrical current, I, flows through an armature coil and the motor then rotates. The equation of the motor is.

$$V = L_m\dot{I} + K_V\omega + R_mI \quad (1)$$

There are three variables, voltage, V, current, I, and motor speed, ω. This means that the resulting current, I, depends not only on the voltage, V, but also on the speed, ω. A permanent magnet DC motor uses a rare earth magnet to provide a strong magnetic field and thus the resulting torque is proportional to the current, I, flow through the motor coil. The torque, T, generated by the motor can be derived from the motor's electrical current, I, as

$$T = K_TI \quad (2)$$

If the applied voltage, V, is commanded and the motor speed, ω, is monitored in real time, the output torque, T, can be approximated by the mathematic model described in Equation (1-2).

The electrical motor normally runs at high speed but only provides a small output torque. Transmission is required to provide mechanical advantages that lower the speed and higher the output torque with the same power rating. In this case, a mechanism to convert the rotational motion of the motor into a linear motion that can drive syringe pistons is needed. Note that syringes are in cylindrical and their pistons are movable in pure translation. In the proposed design, a ball screw is selected since it provides mechanical advantages and at the same time converts the motor's rotational motion into a linear motion. A flexible coupling is used to connect the output shaft of the motor to the shaft of the ball screw to free other axes except in the rotational axis where both shafts are interfaced. In this design, the ball screw provides a rigid coupling between the shaft of the motor to the linear motion of the piston. A feed position of the piston, x_1, can be derived by the kinematic relationship of the ball screw [18]:

$$x_1 = r\tan(\alpha)\,\theta \tag{3}$$

Although the screw provides favorable over-motion conversion and mechanical advantage, it comes with unavoidable friction between the relative surfaces of a nut and a screw. Note that this friction has the properties of asymmetric, hard-nonlinear, time-variant, and sensitive to disturbance [18]. This complication is amplified as the point at which friction occurs is in between the rotational and translational domains. For this reason, the influence of the screw has asymmetric effects on the dynamic of the rotational and translational sides [18].

The coulomb friction model is used for representing the friction in a screw. Then, the angle of friction, γ, can be written in the form of coulomb coefficient, μ, as

$$\gamma = \begin{cases} -\tan^{-1}(\mu)\,; backward\ drive \\ \tan^{-1}(\mu)\,; forward\ drive \end{cases} \tag{4}$$

It is noted that γ can be varied by following the driving direction of the mechanism [18]. Thus, the equation of motion of the carriage can be defined as

$$\left(Mr\tan(\alpha+\gamma)+\frac{1}{r\tan(\alpha)}\right)\ddot{x}_1 = T - Fr\tan(\alpha+\gamma) \tag{5}$$

If the motion of the system is a cause of the effort from the rotation of the screw, the direction is called forward drive. Vice versa, if the effort from the nut drives the system, the direction is backward. It is good to note that the mechanical advantage varies depending on the driving direction whereas the backward driving delivers more mechanical advantage. The reason behind this effect is the interaction of non-linear behavior in screw and friction. By operating in a backward drive, the negative value of γ reduces the value of $\alpha+\gamma$ inside the tangent function. This reduction reduces the influence of load F giving the behavior of higher mechanical advantage. Noted that, in small a lead angle α screw, the effect of negative γ is large enough such that $\alpha+\gamma$ is zero or negative. This effect prevents the effect of action on the nut-side to the system which is called non-back drivable. The screw that possesses this behavior has the ability to self-locking.

The loaded material is typically a viscoelastic material its behavior is the blend between viscous fluid and elastic solid. There are two material properties that are used to precisely control the flow of the material. The first one is elastic modulus which explains the elastic response of the material, and the second one is viscosity which describes the resistance of a fluid to flow. The fluid aspect of viscoelastic material that is mostly used in LDM is non-Newtonian fluid [2], where the relationship between shear rate and shear stress is non-linear. Thus, it makes the resistance of the flow non-linearity.

For the aspect of modeling, the lumped element model is used to describe the material. The elasticity is represented by a spring whose spring constant k corresponds to the elastic modulus of the material. The viscous element could be modeled as a damper with a nonlinear damping coefficient $c(\dot{x}_2)$ corresponding to the viscosity where the x_2 is a motion of material that entering the nozzle. Assuming that the elastic behavior is dominated only in the syringe while only the viscous effect is mainly presented in the nozzle. And the small amount of extruded mass is neglected. The spring is connected

to the damper in series, with a mass of the material that is inside the nozzle, *m*, attached between them.

Let the displacement of material that is entering the nozzle be x_2. The load that acts as a piston can be defined by the spring effect inside the syringe as

$$F = f + k(x_1 - x_2) \tag{6}$$

where *f* is overall friction which resists the system's motion. The equation of motion could then be derived as follows:

$$m\ddot{x}_2 = \mathrm{k}(x_1 - x_2) - \mathrm{c}(\dot{x}_2)\dot{x}_2 \tag{7}$$

where $c(\dot{x}_2)$ is a non-linear damping coefficient:

$$c(\dot{x}_2) = c_1 + c_2\, sgn\,(\dot{x}_2)\,\dot{x}_2 \tag{8}$$

With all the governing Equations (1-8) presented, the stability analysis of the system was analyzed. Lyapunov's second method was used to guarantee the stability of a nonlinear dynamical system.

Let's set the Lyapunov candidate function [19], $\Upsilon(X)$ as a summation of the kinetic energy of the screw and material, electrical energy in the motor, and the energy from viscoelastic material deformation.

$$\Upsilon(X) = \frac{k\,(x_1 - x_2)^2}{2} + \frac{L_m\, I^2}{2} + \frac{m_t\ \dot{x}_1{}^2}{2} + \frac{m\dot{x}_2{}^2}{2} \tag{9}$$

Such function is in a quadratic form which hold the condition of stable point: $\Upsilon(0) = 0$ and the positive definition: $\Upsilon(X) = 0$ if $X \neq 0$.

The derivative form of candidate function is derived as follows.

$$\dot{\Upsilon}(X) = J_t\,\ddot{x}_1\,\dot{x}_1 + k\,(\dot{x}_1 - \dot{x}_2)\,(x_1 - x_2) + m\,\ddot{x}_2\,\dot{x}_2 + L_m\, I\,\dot{I} \tag{10}$$

The derivative form of candidate function with substitution of Equation (1-7) where voltage $V = 0$ is written as.

$$\dot{\Upsilon}(X) = -R_m I^2 - c(\dot{x}_2)\ \dot{x}_2{}^2 - f\dot{x}_1 - \left(\frac{K\,I\,\dot{x}_1}{r\ tan(\alpha)} - \frac{K\,I\,\dot{x}_1}{r\ tan(\alpha+\gamma)}\right) \tag{11}$$

To prove Lyapunov's stability [19], the state must converge to stable point so that $\dot{\Upsilon}(X) < 0$. Noted that, for case of asymptotic stability, such conditions must hold true for $X \neq 0$.

The first term $R_m I^2$ is a power loss in resistor which trivially positive.

The second term $c(\dot{x}_2)\ \dot{x}_2{}^2$ is a loss in non-linear damper.

$$c(\dot{x}_2)\dot{x}_2{}^2 = (c_1 + c_2\, sgn\,(\dot{x}_2)\,\dot{x}_2)\dot{x}_2{}^2 \tag{12}$$

By expanding $sgn\,(\dot{x}_2)$, the term can be written as

$$c(\dot{x}_2)\dot{x}_2{}^2 = c_1\dot{x}_2{}^2 + c_2\,\frac{\dot{x}_2{}^4}{|\dot{x}_2|} \tag{13}$$

Thus, it is proved to be positive for $\dot{x}_2 \neq 0$.

Consider the friction loss $f\dot{x}_1$, the direction of friction always resists the motion of x_1, thus a coulomb viscous friction where its model is written as

$$f = sgn(\dot{x}_1)|f| = \frac{\dot{x}_1}{|\dot{x}_1|}|f| \tag{14}$$

Thus, the $f\dot{x}_1$ can be derived as

$$f\dot{x}_1 = \frac{\dot{x}_1{}^2}{|\dot{x}_1|}|f| \tag{15}$$

This term is always positive.

Considering the fourth and fifth terms as follows.

$$\frac{K\,I\,\dot{x}_1}{r\ tan(\alpha)} - \frac{K\,I\,\dot{x}_1}{r\ tan(\alpha+\gamma)} = \frac{K\,I\,\dot{x}_1}{r}\cdot\left(\frac{tan(\alpha+\gamma) - tan(\alpha)}{tan(\alpha)\,tan(\alpha+\gamma)}\right) \tag{16}$$

The friction angle γ is varied according to the direction of the driving: forward and backward drive. This direction can be assumed to be dependent on energy flow of the screw. The flow of energy is a motion and effort that screw shaft perceive. The power of motor that can be represented as $K\,I\,\dot{x}_1$ can be an indicator of driving direction as a motor is rigidly attached to screw. The positive of $K\,I\,\dot{x}_1$ meaning the motor gives power to the system. So, the screw is in forward drive. Thus, the friction angle can be written case-wise.

$$\gamma = \begin{cases} -\gamma_{abs} & ;\ K\,I\,\dot{x}_1 < 0 \\ \gamma_{abs} & ;\ K\,I\,\dot{x}_1 > 0 \end{cases} \tag{17}$$

In case of $K\,I\,\dot{x_1} < 0$

$$\left(\frac{tan\left(\alpha-\gamma_{abs}\right)-tan(\alpha)}{tan(\alpha)\,tan\left(\alpha-\gamma_{abs}\right)}\right) < 0 \qquad (18)$$

And when $K\,I\,\dot{x_1} > 0$,

$$\left(\frac{tan\left(\alpha+\gamma_{abs}\right)-tan(\alpha)}{tan(\alpha)\,tan\left(\alpha+\gamma_{abs}\right)}\right) > 0 \qquad (19)$$

From those two cases, the sum of these two terms is always positive.

$$\frac{K\,I\,\dot{x_1}}{r\,tan(\alpha)}-\frac{K\,I\,\dot{x_1}}{r\,tan(\alpha+\gamma)} > 0 \qquad (20)$$

Overall, all the four terms in derivative of Lyapunov candidate function are always negative. Therefore, at any initial state X, the system converges to stable because existence of component in which the energy is removed. Thus, the energy that is stored in the system is always reduced.

After the stability of the system is discussed, the ability to sense and control both the pressure and volumetric flow rate of the material are presented as follows:

Since the friction in the screw is coulomb viscous friction, if the motor rotates and the piston pushes the material to flow out, the friction is kinetic friction. Both the pressure, P, and the volumetric flow rate, Q, are visible at the actuator's side. But when the motor and the piston stops and flow ceases, the friction is in static friction. The friction behavior is in the dead-band and the pressure, P, is invisible to the actuator's side.

The force pushing the material through the nozzle is analogous to the force exerted by the spring which is equal to F - f. The pressure of the material at the nozzle entrance, P, can be derived as

$$P = \frac{4(F-f)}{\pi D^2} \qquad (21)$$

Equation (1-5) shows that the force at the piston, F, can be calculated from the controllable voltage, V, and the measured motor's position, θ. The force can then be used in Equation (6) and (21) to obtain the volumetric flow rate, Q, (directly proportional to x_2) and pressure, P, respectively. This proves that by measuring and controlling only two variables, the applied voltage, V and the motor's position, θ, both the pressure, P, and volumetric flow rate, Q, of the system can be derived and manipulated at any given time. However, since both are directly affected by the same variables, only one of them can be controlled at a time.

$$P = \frac{4\left(\frac{K_T\,(V-K_V\omega)}{R_m}-f\,r\,\tan(\alpha+\gamma)\right)}{D^2\,r\,\pi\,\tan(\alpha+\gamma)} \qquad (22)$$

Furthermore, the elastic behavior of the material is disregarded at the steady state, meaning that the rate of change for x_1 and x_2 are coupled. Thus, the volumetric flow rate, Q, of the material can then be derived from the motor's speed, ω, via Equation (3). By applying the closed-loop controller over the measured motor's position, θ, the steady state volumetric flow rate, Q, can be directly handled. Similarly, at the steady state, the pressure P is coupled to and can be controlled by only varying the voltage, V. It is also important to note that the pressure inside the nozzle is the gradient from the pressure, P, to the atmospheric pressure.

$$Q = \frac{\pi\,D^2\,\dot{x_2}}{4} \qquad (23)$$

Rearrange all the equations, the volumetric flow rate, Q, is approximated at the steady state from the motor's speed, ω, as

$$Q = \frac{\pi\,D^2\,r\,tan(\alpha)\,\omega}{4} \qquad (24)$$

The pressure, P, and the volumetric flow rate, Q, at the steady state is thus determined from (1) the applied voltage, V, (2) the time derivative of the motor's position, θ, and (3) the model.

It is favorable to handle both the pressure, P, and the volumetric flow rate, Q, to enhance the printing process [20]. The flexible actuation technique is an excellent candidate to control the flow of the material and may unlock the technique we handle the printing process.

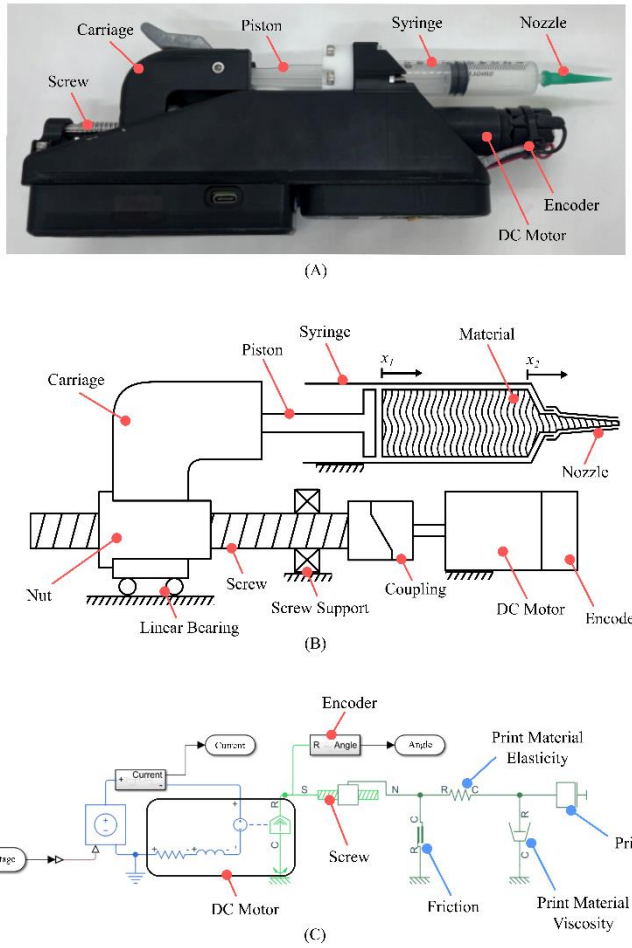

Fig 2 A ram-extruder with flexible actuation and intrinsic sensing for 3D printing, (A) Fabricated hardware, (B) Schematics, (C) Bond Graph Diagram.

2.2 Material Properties Sensing

Apart from the pressure, P, and the volumetric flow, Q, the intrinsic sensing feature also allows the extruder to sense the material properties. In this simulation, the detection of the material viscosity, $c(\dot{x_2})$, is demonstrated. Combining Equations (1-7), $c(\dot{x_2})$ in the steady state can be determined as

$$c(\dot{x_2}) = \frac{\left(V_t - K_V\omega(t)\right)\frac{K_T}{R_m} - fr\tan(\alpha+\gamma)}{r^2\tan(\alpha+\gamma)\tan(\alpha)\omega(t)} \quad (25)$$

In the steady state, where applied voltage, V, is controlled, the motor's speed, ω, is calculated (from the measured motor's position, θ), and all intrinsic parameters a *priori* are known. Equation (25) demonstrates the proposed model's ability to sense the damping coefficient, c, of the damper used in the model, which represents the viscosity of the material. The proposed ram extruder was simulated with the MATLAB Simscape model (Fig 2C). Such model was constructed with the bond-graph approach [21], where each element is interfaced with both effort and flow signals. The parameters of the simulation can be found in Table 1.

To validate the measurement of the viscosity, the applied voltage, V, was applied at various constant levels of 8, 10, and 12V. Materials whose damping coefficients were unknown to the system were tested. The damping coefficient of these material spanned in

the range of 0 to 10,000 N·s/m with 1000 N·s/m increments.

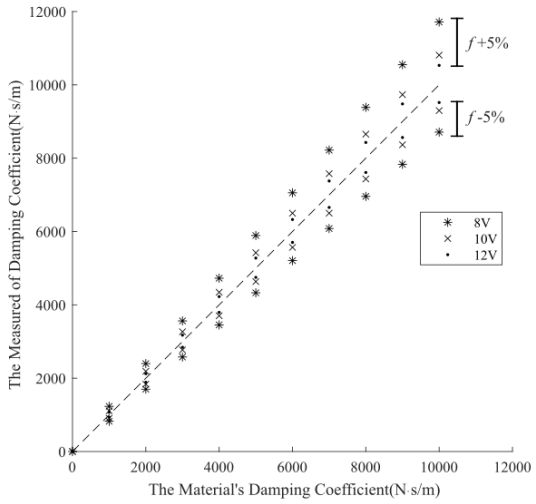

Fig 3 The simulated result of the damping coefficient measurement. The dotted diagonal line represents the correct estimation. The data above this line are the result of the input friction error of +5%, and the data below this line are from the friction error of -5%.

The motor's speed, ω, is obtained to predict the damping coefficient of the loaded material through Equation 10. In case that the parameter in the system is imprecisely modeled, a simulation is used to demonstrate that the technique is still effective. In the following simulation, the friction is assumed to be imprecisely modeled with ±5% error. The deviation, resulting from an error in the friction input, is proportionally constant for different values of the damping coefficient. Which +5% friction error results in the guesses higher than the input values and vice versa for -5%. The higher voltage suggests lower deviation and more immunity to the change of hardware parameters.

2.3 Hardware Description

A custom extruder print head (Fig 2a) was designed and fabricated based on the proposed concept. The Faulhaber DC motor 2342S024CR with magnetic encoder IE3-1024 L was selected as the actuator. It was connected to the THK ball screw BNK0802 via a flexible coupling. The chassis and other passive components of the extruder were 3D printed using SLA resin. It was designed so that a 10-mL syringe main body can be clamped on the chassis while the syringe piston movement is coupled with the ball screw nut.

The custom-designed PCB was used to control the extruder hardware. It utilizes a DRV8876PWPR DC motor driver chip which features the current sensing ability, allowing the real-time measurement of electrical current supplied to the motor. The STM32 based microcontroller was employed to handle the communication and signal processing. Its firmware was specially designed to switch between constant voltage mode (pressure-controlled) and closed-loop mode (volumetric-controlled). In the closed-loop mode, a proportional–derivative controller was applied to precisely manipulate the motor movement. The motor position and the electrical current reported from the microcontroller were logged over time for usage in the experiments. The size of the assembly without the syringe is roughly 220x110x50 mm and its weight is 622 grams. The maximum power is 24 Watts. This gives the maximum pressure exceeding 7 Bars and maximum volumetric flow of approximately 6 mL/s at no load.

This ram extruder was designed to connect and communicate with consumer 3D printers via a specially designed adapter. The adapter transmits the STEP/DIR/EN signal normally used for stepper-based extruders in typical Fused Deposition Modelling printers. In the closed-loop extrusion, this custom extruder receives these signals from the printer and controls the extrusion at the rate of the STEP signal. The adapter also relays the serial communication for the extruder, allowing the usage of the special G-CODE commands, and the recording of the extruder data, including piston position and electrical current.

2.4 Experiment Setup

2.4.1 Print Materials

To demonstrate the proposed flexible extrusion profiles and intrinsic sensing of the ram extruder, three materials, (a) biogel (5% food-grade gelatin solution), (b) chocolate fudge, and (c) silicone sealant have been chosen. These materials are viscoelastic material that can be 3D printed using the Liquid Deposition Modeling (LDM) technique. Each material represents different fields in which LDM technology provides useful applications, including (a)

tissue engineering, (b) food, and (c) engineering respectively. These materials also exhibit different flow behaviors which illustrate how this proposed system will perform on various materials in real-world applications with distinct rheological properties.

2.4.2 Flexible Actuation

In this section, experiments were designed to demonstrate the different outcome between the pressure-controlled and volumetric-controlled modes. The behavior of the print material during (a) flushing and (b) printing operations has been conducted, analyzed, and compared.

Firstly, the flushing process of chocolate fudge was performed six times. In the first half, different controlled feed rates of 1, 2, and 3 mm/s were executed. Then, the controlled pressures at the motor voltage of 8, 10, and 12V were implemented for the second half. To equalize the amount of material extruded for each attempt, all extrusion was halted when the piston position of 3 mm from the starting point is reached. In other words, about the same amount of material was used in each test. The motor's position, θ, and the motor's electrical current, I, were measured over time by the encoder and the motor driver chip respectively.

Secondly, all three materials mentioned above were used to lay 30 mm long lines. For each material, four lines were printed, first with volumetric-controlled extrusion mode at the volumetric feed rate of 4.17 mm^3/s (This feed rate provides the cross-sectional area of the line at 0.5 mm^2), and the remaining with pressure-controlled extrusion mode at the motor voltage at 6, 8, and 10V. All lines were laid at the nozzle height of 0.5 mm and horizontal feed rate of 3000 mm/second. This study is focused on the steady-state line properties; thus the 60 mm long square-wave-shaped line was printed immediately before the experimental lines. The pictures of glass slides on which lines were printed and then taken through a telecentric lens. The extraction process of mean and standard deviation of the line widths is shown in Fig 4. The image analysis was used to determine the quanlity of the printed line.

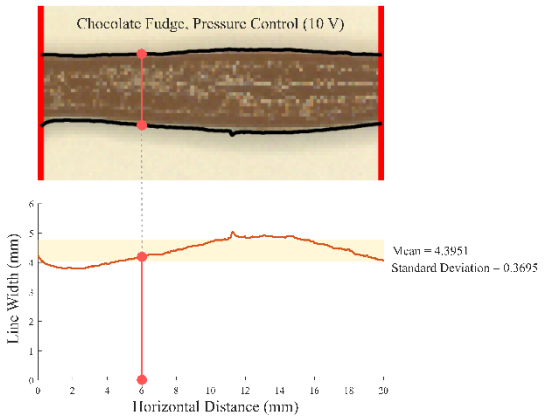

Fig 4 Line width extraction process. The pictures of the lines are processed using a binary thresholding technique to find the upper and lower bounds of the lines. Then the numbers of pixels between the upper and lower bound at the same vertical position are counted. These numbers are obtained along the selected portion of the printed lines. The mean and standard deviation of these numbers are then calculated.

2.4.3 Intrinsic Sensing

Apart from utilizing flexible actuation, the sensed pressure, P, and volumetric flow rate, Q, can be used to perceive the properties of the print materials. The ability to perceive real-time properties of the print material was validated through a heterogenous mixture extrusion test. The syringe containing the mixture was prepared as shown in Fig 5. The volumetric-controlled extrusion was then executed on this non-homogenous mixture at the reference piston feed rate of 3600 mm/second, while the piston feed rate was logged over time together with motor's electrical current, I, which can be used to validate the motor torque, T.

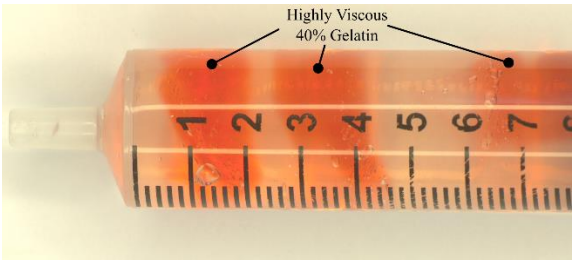

Fig 5 The heterogenous mixture of 40% food-grade gelatin in water solution (red) deposited in its 5% counterpart (clear). The mixture is stored in the syringe.

3. Result and Discussion

3.1 Flexible Actuation: Flushing Process

The measured motor current, *I*, and piston feed rate from the pressure-controlled and volumetric-controlled flushing of chocolate fudge are shown in Fig 6. The piston feed rate was calculated from the differentiation of the measured piston position over time, and the motor current, *I*, can represent the torque, *T*, generated from the motor and correspond with the pressure, *P*, in the steady state.

In the pressure-controlled flushing process, the constant voltage, *V*, applied to the motor and the piston initialized the flow of the print material from its resting state. This results in the surge of the motor's electrical current, *I*, to certain values. The current, *I*, appeared to stabilize around the values until the end of the process. Implies that the torque, *T*, exerted by the motor was stabilized around a certain value depending on the applied voltage, *V*. The elasticity of the material caused the piston feed rate to experience a high magnitude of fluctuation at first, then the feed rate gradually slowed down at a different rate depending on the applied voltage, *V*.

In the volumetric-controlled flushing process, after the motor current, *I*, displays a relatively slower rise, the complex behavior of material elasticity and viscosity triggers a large magnitude of fluctuation in the electrical current with diverse behavior depending on the applied feed rate. The current from each feed

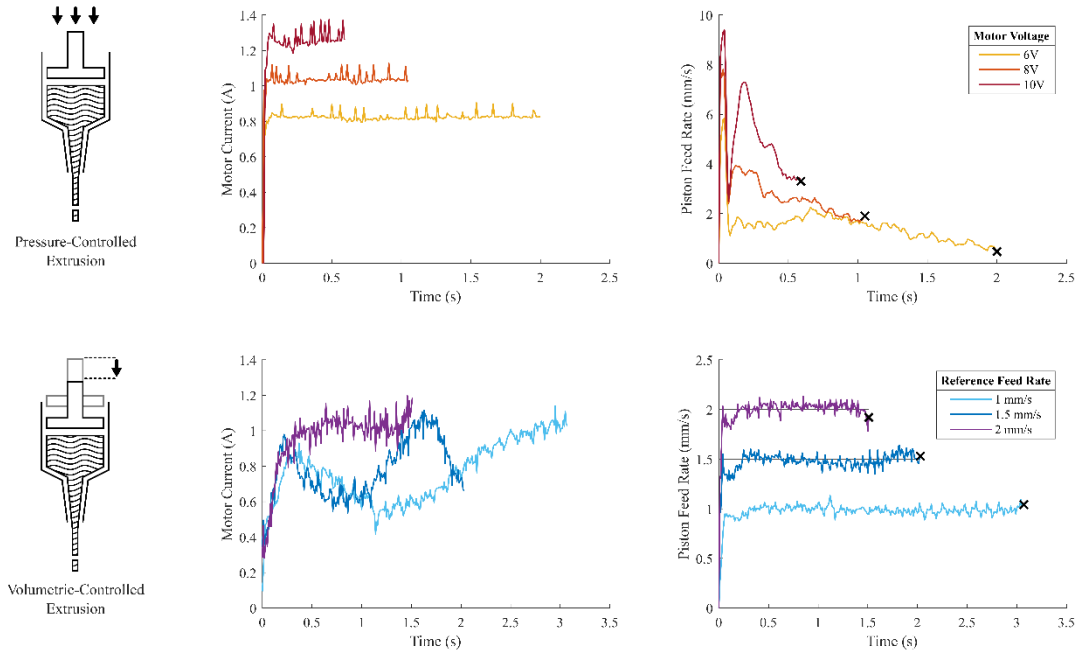

Fig 6 Experiment data from the flushing operation of different modes. Pressure-controlled Extrusion (Top) is actuated by 8, 10, and 12 V. Volumetric-controlled Extrusion (Bottom) is commanded at the piston's reference feed rate of 1, 2, and 3 mm/s. All extrusion ends when a piston displacement of 3 mm is reached, this point is marked by the black "X".

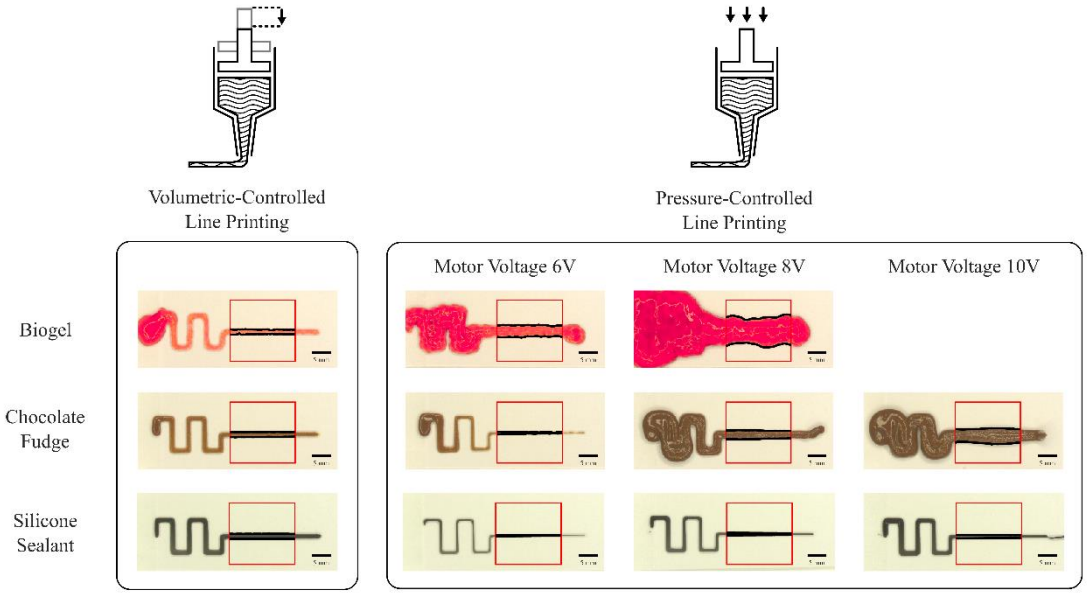

Fig 7 The printed lines using volumetric-controlled and pressure-controlled extrusion. The selected region is indicated by red squares. These are area which mean and standard deviation of line width are extracted. The black scale bar in pictures is 5mm in length.

rate did not appear to converge to any certain value in the 3 mm extrusion time frame. On the contrary, after slight instability, the feed rate of the piston continues to stabilize around the controlled reference value.

3.2 Flexible Actuation: Line Printing

Three materials used for printing exhibited different flow behavior and magnitude of deformation resistance. Silicone sealant displays the highest viscosity followed by chocolate fudge, and biogel respectively. The pictures of the printing results of these materials under both extrusion modes are displayed in Fig 7. The mean line width and standard deviation of line width were extracted from each printed line and are shown in Table 3.

In each particular material, the mean line width shows a positive correlation with the motor voltage, V. However, the magnitude and the rate of change were diverse with respect to the viscosity of the materials. At every particular voltage, V, silicone sealant was found to have the minimum mean line width followed by chocolate fudge, and biogel, while the difference between the smallest and greatest value was in the order of millimeters, in contrast to volumetric-controlled printing, where each material's mean line width spanned in the range of hundreds of microns.

Correspondingly, a positive correlation with voltage was found for the standard deviation. However, the correlation displays worse linearity than those of the mean line width. At each voltage, V, the standard deviation also displays similarity to the mean, with the lowest deviation presented in silicone sealant presenting the domination of its viscosity over its elasticity. The highest deviation was found in

Table 3 Mean Line Width(μ) in the unit of mm with Standard Deviations(σ). The lowest standard deviation value for each material is indicated by [1]

	Position Controlled		Pressure Controlled					
			Motor Voltage 6V		Motor Voltage 8V		Motor Voltage 10V	
Materials	μ	σ	μ	σ	μ	σ	μ	σ
Biogel	1.4254	0.1080[1]	3.4999	0.1890	8.4479	0.6639	N/A	N/A
Chocolate Fudge	1.5267	0.0394[1]	0.4972	0.1683	2.5965	0.1945	4.3951	0.3695
Silicone Sealant	1.5531	0.0142[1]	0.2866	0.0347	0.6574	0.0665	0.9613	0.0725

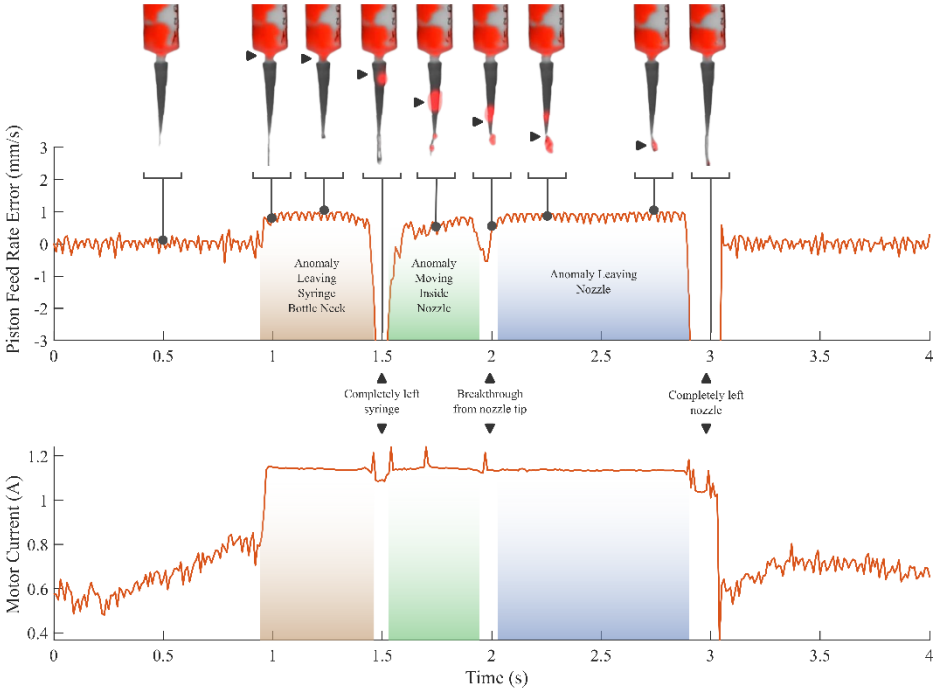

Fig 8 The illustration of intrinsic sensing: visibility of printing material. Anomaly-infested material is represented by a non-homogenous biogel formed by mixing concentrated biogel (red) in its regular counterpart(transparent). Piston feed rate error is calculated from the difference between the reference feed rate and the actual feed rate measured by the encoder. The trend of this parameter corresponds with the location of the anomaly which is illustrated by black triangles. The motor current is measured by the motor driver chip and is proportional to the force that the motor exerts.

biogel where its dominant elasticity caused the wobbling in the printed line. This trend occurred similarly in volumetric-controlled printing. It is also important to note that, for every material, the smallest standard deviation was encountered when printed in volumetric-controlled mode.

3.3 Intrinsic Sensing: heterogenous mixture extrusion

In this experiment, a non-homogenous hydrogel mixture was extruded using the proposed technique and machine vision was used to capture the flow during extrusion. The video was synchronized with the signals monitored from the ram extruder's microcontroller. Throughout the extrusion of a non-homogenous hydrogel mixture, piston feed rate error and motor current were plotted over time as shown in Fig 8.

At the beginning of the extrusion, regular hydrogel flowed through the nozzle and escaped at the nozzle tip. The feed rate error was stabilized around the value of 0 mm/s while the motor current slowly rose. At around 1 second, a small part of the highly concentrated gel was forced through the narrow area at the lowest section of the syringe. Due to its much greater viscosity, the same stress applied could not maintain the constant flow of the material anymore. Thus, the feed rate error and motor current sharply increased to around 1 mm/s and 1.2A respectively. During the next 0.5-second period, more volume of the viscous gel was constantly pushed through the syringe bottleneck, corresponding with the steadiness of the two variables at the raised values. At roughly 1.5 seconds, the concentrated fragment detached from the main body and slipped into the broadest part of the nozzle (uppermost). When the viscosity of the material at the bottleneck sharply drops, the internal stress of the material in the syringe is instantly released. The residual gel in the nozzle is rapidly pushed out at the tip. This overflow results in a drastic drop in feed rate error and a small drop in

motor current. The detached then drifted down toward the tip of the nozzle. More effort from the motor is required to push it through the smaller cross-sectional area. Hence, the feed rate error slowly increased while the motor current was steady at the elevated level.

At roughly 2 seconds, part of the fragment has begun to escape through the nozzle tip. This process has been continued for almost 1 second, while both feed rate error and motor current were maintained at the ascended values. At around 2.9 seconds, the fragment of concentrated gel fully departed from the nozzle tip. The instant pressure release and the overflow of the material out of the nozzle cause a sharp drop in the feed rate error together with a small drop in motor current, followed by a rapid decrease at the next 0.2 seconds, approximately. without the presence of highly viscous gel in the syringe bottleneck and the nozzle, the feed rate error once again converged around the value of 0mm/s, while the motor current dropped back and slightly fluctuated around 0.7A. The proposed intrinsic sensing can be further developed to gain insight into the flow, e.g., anomaly detection.

In the actual case of viscoelastic material, the flow is highly complex as the material possesses both properties of solid and fluid. The material needs to be compressed through the taper of nozzle. The deformation and the flow of matter are very difficult to model. Furthermore, it is sensitive to disturbances such as temperature. Noted that, even if the temperature is controlled, it is still challenging to guarantee the temperature everywhere inside the syringe is identical. This complication of rheology may reflect the pressure and flow.

In the demonstration, the proposed prototype can detect the difference in rheology as the material suddenly gains more viscosity and stiffness. The results (Fig 8) show the potential usage of the thresholding method to detect clogging inside the nozzle. In the graph, the piston feed rate error of 0.5 mm/s can be used to detect anomalies. This detection may further be used in real applications to prevent print failure.

Furthermore, the signal that is demonstrated in Fig 8 also reflect the flushing completion where the clog is flushed out. The drastic drop of feed error is highly related to the breakthrough of the clog. This event is easily detected using threshold technique. Combining with the clogging detection, the proposed hardware has a potential to detect clog real-time during printing process and also able to sense the completion of clog flushing.

3.4 Discussion

The greater repeatability of material extrusion could be achieved by ensuring the initial conditions of the flow. Unlike purely elastic or purely viscous materials, viscoelasticity exhibits the exponential relaxation of stress over time. The difference in initial residual stress will affect the flow behavior of the material. Thus, starting the process from the same internal pressure is favorable. The experiment illustrates that relatively higher-pressure stability could be attained by utilizing constant voltage driving. Arguably, the internal pressure from the volumetric-controlled flushing process might converge at some point. Yet, the time required for this to occur is proven to be significantly longer.

In contrast, line laying with a pressure-based actuation approach could be challenging. The characteristics of printed lines are proven to be profoundly affected by the viscosity and elasticity of the material. The viscosity describes the deformation rate of the material when stress is applied, it dictates the amount of material extruded at a certain pressure, thus governing the mean width of the printed line. In the mass spring damper system, the higher spring constant results in a larger amplitude and frequency. Similarly, materials with higher elastic modulus can store more residual stress resulting in higher deviation in the width.

The control of line width is hardly possible without intensive calibration of the print pressure on the material. Moreover, the change in the material viscosity caused by time, temperature change, and chemical reactions could influence the conditions of the printed line [22]. At a steady state, higher resilience on material properties is shown to be achieved by manipulation of the piston position rather than the internal pressure of the material. The volumetric-controlled extrusion method demonstrates greater reliability and superior uniformity of the line width.

The material sensing capability was demonstrated in the last experiment. The measured response suggests that the system successfully distinguishes between regular and highly viscous gel while it

travels through the syringe bottleneck and the nozzle. This suggests that the viscosity of the material can be sensed by the proposed hardware as demonstrated in the simulation.

With proper calibration, the proposed design might be able to sense the properties of an unknown material stored in the syringe and adjust the printing profile accordingly to the material. The ability to detect and resolve unexpected anomalies might also be possible if the change in viscosity is present. For example, re-printing of the disconnected line caused by bubbles in the material, and mid-print flushing when the sediment is detected in the nozzle.

4 Conclusion

The proposed flexible actuation system with intrinsic sensing can control the flow in two modes: pressure control and volumetric control. Since the overall system is in nonlinear dynamics with friction, pressure control gives a better desired pressure whereas volumetric control gives a better precision flow. Actuation-sensing mechanism is also proposed such that the pressure and flow rate are sensible from the actuator's side. In the pressure control mode, the volumetric flow is real-time sensible. Vice versa, in the volumetric flow mode, the pressure is real-time monitored. With this capability, the loaded material's properties can be revealed during actuation. This provides a foundation for further development and optimization of flexible actuation systems for 3D printing.

5 Reference

[1] A. D. Valino, J. R. C. Dizon, A. H. Espera, Q. Chen, J. Messman, and R. C. Advincula, "Advances in 3D printing of thermoplastic polymer composites and nanocomposites," *Prog Polym Sci*, vol. 98, p. 101162, Nov. 2019, doi: 10.1016/j.progpolymsci.2019.101162.

[2] J. A. Lewis, "Direct Ink Writing of 3D Functional Materials," *Adv Funct Mater*, vol. 16, no. 17, pp. 2193–2204, Nov. 2006, doi: 10.1002/adfm.200600434.

[3] A. D. Valino, J. R. C. Dizon, A. H. Espera, Q. Chen, J. Messman, and R. C. Advincula, "Advances in 3D printing of thermoplastic polymer composites and nanocomposites," *Prog Polym Sci*, vol. 98, p. 101162, Nov. 2019, doi: 10.1016/j.progpolymsci.2019.101162.

[4] Q. Chen, P. Cao, and R. C. Advincula, "Mechanically Robust, Ultraelastic Hierarchical Foam with Tunable Properties via 3D Printing," *Adv Funct Mater*, vol. 28, no. 21, May 2018, doi: 10.1002/adfm.201800631.

[5] G. M. Gratson, M. Xu, and J. A. Lewis, "Microperiodic structures: Direct writing of three-dimensional webs," *Nature*, vol. 428, no. 6981, pp. 386–386, Mar. 2004, doi: 10.1038/428386a.

[6] A. M'Barki, L. Bocquet, and A. Stevenson, "Linking Rheology and Printability for Dense and Strong Ceramics by Direct Ink Writing," *Sci Rep*, vol. 7, no. 1, p. 6017, Jul. 2017, doi: 10.1038/s41598-017-06115-0.

[7] S. J. Kalita, S. Bose, H. L. Hosick, and A. Bandyopadhyay, "Development of controlled porosity polymer-ceramic composite scaffolds via fused deposition modeling," *Materials Science and Engineering: C*, vol. 23, no. 5, pp. 611–620, Oct. 2003, doi: 10.1016/S0928-4931(03)00052-3.

[8] S. Hong, C. Sanchez, H. Du, and N. Kim, "Fabrication of 3D Printed Metal Structures by Use of High-Viscosity Cu Paste and a Screw Extruder," *J Electron Mater*, vol. 44, no. 3, pp. 836–841, Mar. 2015, doi: 10.1007/s11664-014-3601-8.

[9] A. E. Jakus, S. L. Taylor, N. R. Geisendorfer, D. C. Dunand, and R. N. Shah, "Metallic Architectures from 3D-Printed Powder-Based Liquid Inks," *Adv Funct Mater*, vol. 25, no. 45, pp. 6985–6995, Dec. 2015, doi: 10.1002/adfm.201503921.

[10] J. Malda *et al.*, "25th Anniversary Article: Engineering Hydrogels for Biofabrication," *Advanced Materials*, vol. 25, no. 36, pp. 5011–5028, Sep. 2013, doi: 10.1002/adma.201302042.

[11] D. N. Heo *et al.*, "3D Bioprinting of Carbohydrazide-Modified Gelatin into Microparticle-Suspended Oxidized

Alginate for the Fabrication of Complex-Shaped Tissue Constructs," *ACS Appl Mater Interfaces*, vol. 12, no. 18, pp. 20295–20306, May 2020, doi: 10.1021/acsami.0c05096.

[12] D. B. Kolesky, R. L. Truby, A. S. Gladman, T. A. Busbee, K. A. Homan, and J. A. Lewis, "3D Bioprinting of Vascularized, Heterogeneous Cell-Laden Tissue Constructs," *Advanced Materials*, vol. 26, no. 19, pp. 3124–3130, May 2014, doi: 10.1002/adma.201305506.

[13] S. Khalil and W. Sun, "Biopolymer deposition for freeform fabrication of hydrogel tissue constructs," *Materials Science and Engineering: C*, vol. 27, no. 3, pp. 469–478, Apr. 2007, doi: 10.1016/j.msec.2006.05.023.

[14] D. G. Karis *et al.*, "Cross-linkable multi-stimuli responsive hydrogel inks for direct-write 3D printing," *Polym Chem*, vol. 8, no. 29, pp. 4199–4206, 2017, doi: 10.1039/C7PY00831G.

[15] N. E. Fedorovich *et al.*, "Evaluation of Photocrosslinked Lutrol Hydrogel for Tissue Printing Applications," *Biomacromolecules*, vol. 10, no. 7, pp. 1689–1696, Jul. 2009, doi: 10.1021/bm801463q.

[16] C. Mandrycky, Z. Wang, K. Kim, and D.-H. Kim, "3D bioprinting for engineering complex tissues," *Biotechnol Adv*, vol. 34, no. 4, pp. 422–434, Jul. 2016, doi: 10.1016/j.biotechadv.2015.12.011.

[17] D. O. Kazmer, S. Kodra, A. A. Mubasshir, E. E. Keaney, and J. L. Mead, "Additive ram material extrusion and diddling of fully compounded thermoset nitrile rubber," *Polym Compos*, vol. 42, no. 10, pp. 5237–5248, Oct. 2021, doi: 10.1002/pc.26218.

[18] O. Vahid-Araghi and F. Golnaraghi, *Friction-Induced Vibration in Lead Screw Drives*. New York, NY: Springer New York, 2011. doi: 10.1007/978-1-4419-1752-2.

[19] A. Bacciotti and L. Rosier, *Liapunov Functions and Stability in Control Theory*. Berlin, Heidelberg: Springer Berlin Heidelberg, 2005. doi: 10.1007/b139028.

[20] B. K. Deuser, L. Tang, R. G. Landers, M. C. Leu, and G. E. Hilmas, "Hybrid Extrusion Force-Velocity Control Using Freeze-Form Extrusion Fabrication for Functionally Graded Material Parts," *J Manuf Sci Eng*, vol. 135, no. 4, Aug. 2013, doi: 10.1115/1.4024534.

[21] J. Kypuros, *System Dynamics and Control with Bond Graph Modeling*. CRC Press, 2013. doi: 10.1201/b14676.

[22] K. Li *et al.*, "4D printing of MXene hydrogels for high-efficiency pseudocapacitive energy storage," *Nat Commun*, vol. 13, no. 1, p. 6884, Nov. 2022, doi: 10.1038/s41467-022-34583-0.